CHAPTER - 3

Conformational study and investigation of intramolecular S-centered H-bonding in Dithiothreitol (DTT)

3.1 Introduction

Dithiothreitol (DTT), also known as Cleland's reagent, is a highly water soluble solid which acts as a reducing agent or protecting reagent for thiols (-SH). It maintains monothiols in its reducing state as well as reduces the disulfide linkages (-S-S-). Because of its low redox potential, DTT does not get easily oxidized in air. Therefore, it has proved to be a much superior thiol compared to other thiols and are widely used as protective reagents for sulfhydryl groups.[1] Whereas it reduces the disulfide bond of proteins and peptides it also prevents the formation of disulfide linkages in cysteine residues.[1] It protects the enzyme activity loss by the oxidation of sulfhydryl groups.[2] It also has been used to enhance/inhibit the enzymes/receptors activity in various instances.[3–10] Many of the molecule's properties (physical, chemical and biological) are governed by conformation of the molecule and therefore having a precise knowledge about the conformational aspects of the molecule becomes important. Besides, the relation between conformational flexibility and their reactivity can also be identified by conformational analysis.[11–13] In case of DTT molecule extensive studies have been carried out to show its biological and chemical application only but its conformational space has not been explored to a significant extent. Hitherto neither an experimental/computational examination of its crystal structure nor a conformational analysis has been carried out except for the crystal structure of its complex with arsenic carried out in 1972 by W. B. T. Cruse et al.[14]

As the structure of DTT molecule contains two -OH and two -SH groups, it is worthwhile to investigate whether intramolecular non-covalent H-bond interactions are possible and therefore could help stabilize the molecule. In addition to oxygen, weak H-bond formations can also be exhibited by carbon, nitrogen, sulfur, and selenium atoms.[15–17] Although Sulfur-centered H-bonding has not been much explored as conventional H-bonding.[18–22] However, because DTT contains both -SH and -OH groups, it would be interesting to evaluate both the donor and acceptor capabilities of S atoms in addition to O atoms for the formation of sulfur-centered intramolecular H-bonds with O atoms

present in DTT itself. Thus to forecast its stability, the study of the aforementioned molecule is crucial from the perspective of sulfur-centered H-bonding.

Considering that computational techniques are highly efficient at predicting the structural, physical, and chemical properties of molecules, the conformational, structural and spectroscopic properties of DTT were explored computationally utilizing ab initio methods in this study. Further calculations like AIM (Atoms in molecule) were carried out to assess the binding energy of weak H-bonds. And NCI (non-covalent interaction) for the visualization of weak non-covalent bonds. NBO (Natural bond orbital) calculations gave information that both oxygen and sulfur atom act as a donor atom to form weak H-bonds. FMO (Frontier molecular orbital), charge calculation, ^{1}H-NMR and vibrational modes analysis were also performed for the titled molecule. The computational results reported in this work were found in good agreement with the earlier reported experimental data.

3.2 Computational And Experimental Details

Gaussian 16 suite of program was used for all the calculations. Relaxed scan was performed at the B3LYP/cc-pVTZ level of theory with step size of 5° variations in all the dihedral angles such as S17-C1-C4-C6, C4-C1-S17-H18, C1-C4-C6-C8 and C6-C4-O11-H12 [atom numbering as per figure 3.2] to generate the potential energy surfaces. Geometry optimization was done at CCSD/cc-pVDZ level of theory. Single point calculations were performed at CCSD(T) levels of theory using cc-pVNZ (where N = D, T, Q) basis sets for all conformers of DTT. Helgaker method was utilized to extrapolate correlation energy, and results were obtained with basis sets cc-pVNZ (where N = T, Q). Population of different conformers was also calculated with the help of Boltzmann distribution equation as mentioned in chapter 2 (section 2.2) of this thesis.

Geometrical parameters and charge analysis were carried out at same level of theory [CCSD/cc-pVDZ]. Electrostatic potential (ESP) mapping was carried out over optimized structure of DTT molecule in order to detect the possible reactive centers in DTT. The intramolecular (H-bond) interactions were investigated by means of Atoms in molecule

(AIM) calculations, NCI (Non-covalent Interaction) calculations and visualized utilizing the Multiwfn software. With the help of natural bond orbital (NBO) calculation the intra-molecular charge transfer, hyperconjugative interactions and their strength was investigated in DTT molecule. Insights about chemical reactivity and stability of molecule was obtained by the frontier molecular orbital (FMO) calculation. With the help of FMO results the calculation of global reactivity descriptors like μ, η, χ and ω (Electrophilicity index) were done utilizing the equations (mentioned in introduction section 1.6.6). For calculation of the maximum absorbance of DTT molecule the TD-DFT method was utilized. And the ^{1}H-NMR spectra was calculated using GIAO method. Harmonic vibrational IR active modes were calculated and were also assigned by visualizing the modes in the Gaussview 6.0.1 platform. CCSD/cc-pVDZ level of theory was utilized for all the above calculations.

DTT (1,4-Dithiothreitol), from Sigma Aldrich, was procured commercially and used as such. Fourier-transformed infrared spectra (FT-IR) were recorded using the Nicolet iS5 instrument manufactured by THERMO Electron Scientific Instruments LLC. For the Raman measurement of solid DTT powder, a 785 nm diode laser was employed as the excitation source, along with a 3648 pixel CCD detector provided by Research India. The Raman measurement utilized a laser power of 0.71 mW and an exposure time of 5 seconds. Raman spectra were subjected to usual processing for background subtraction, noise and cosmic shower removals prior to analyzing them.

3.3 Results and Discussion

3.3.1 Conformational Analysis

The nomenclature of the conformers of DTT adopted herein follows the nomenclature of tetritols (particularly threitols) by A. J. Lopes Jesus et al.[23] Briefly, the conformers were labeled with 3 letters (in upper case), representing the orientation of following dihedral angles: S15-C8-C6-C4, C8-C6-C4-C1 and O11-C4-C1-S17, respectively. The letters used were G (gauche clockwise), G'(gauche anticlockwise) and T(trans) which represents dihedral of 60°, -60° and 180°, respectively, within a tolerance of ±20°. And the backbone

designation was followed by a number that discriminates conformers with the same backbone conformation but differs due to the orientation of OH and SH groups.

The conformational space of DTT was explored by computing the potential energy surface corresponding to all the important dihedral angles (S17-C1-C4-C6), (C4-C1-S17-H18), (C1-C4-C6-C8) and (C6-C4-O11-H12) (Note that the number after the atomic symbol here as well as elsewhere represents the labeling scheme as per Figure 3.2) of this molecule. These dihedral angles were systematically varied in steps of 5° of the 360° complete rotation around the bond at the B3LYP/cc-pVTZ level of theory through a relaxed scan (Figure 3.1). In the individual relaxed scan of the S17-C1-C4-C6 dihedral angle (Figure 3.1a) 3 minima (sans the starting geometry) were observed of which 2 were of nearly same energy and were the least in energy among all other minima, not only from this scan but compared to all other scans as well. These two iso-energic minima were labeled as G'TG'1 and G'TT. Even though the energy of G'TG'1 and G'TT were nearly same, there were significant structural differences between them and the energy barrier was found to be 3.2 kcal/mol. The other local minimum from the same scan was found to be 6.0 kcal/mol higher in energy than the G'TT/ G'TG'1 minima conformers and was named as G'TG. And a similar relaxed scan of the dihedral (C4-C1-S17-H18) angle revealed a local minimum G'TG'2 along with the global minimum G'TG'1 which were separated by a barrier of 4.6 kcal/mol. Similarly, relaxed scan of dihedral (C6-C4-O11-H12) angle revealed G'TG'3 local minima along with G'TG'1 global minimum, which were 4.96 kcal/mol of energy barrier between them. While the dihedral relaxed scan (C1-C4-C6-C8), revealed only local minima named as, G'GG', G'TG'3 and G'G'G'. The energy barrier between G'TG'3 and G'GG' was observed to be 4.3 kcal/mol and between G'G'G' and G'GG' was found to be 5.3 kcal/mol.

It is important to highlight that a distinct abrupt transition was observed in these dihedral angle relaxed scans (Figure 3.1a, 3.1b, and 3.1d). For instance, In S17-C1-C4-C6 and C4-C1- S17-H18 dihedral angle relaxed scan the pronounced leaps in energy levels stem from the heightened stability introduced to the conformer at the 160° dihedral angle. This stability arises from the intramolecular interaction between the S15-H16 and O13

components. In contrast, at a dihedral angle of 155°, the energy is elevated due to repulsion between S15-H16 and H14-O13. Given the nature of these scans as relaxed processes, optimization takes place at every scan increment. Likewise, a distinct transition occurs between conformers at the dihedral angle of 230° to 225°. This is attributed to a reconfiguration of the O13-H14 bond orientation. At the dihedral angle of 225°, the O13 atom is situated towards proton atoms of both O11-H12 and S15-H16 bonds, whereas at a dihedral angle of 230°, this orientation changes leading to H16-S15---H14-O13---H12-O11kind of interaction. which imparts stability to the conformer at the specific dihedral angle of 230°, leading to the observable sharp transition.

Moving forward, in the context of the C4-C1-S17-H18 dihedral angles relaxed scan, a notable pattern emerges. At a dihedral angle of 250°, the high-energy conformer experiences opposing orientations of both the O13-H14 and O11-H12 groups. This configuration induces repulsion between the lone pairs of electrons present in these groups. Contrastingly, at a dihedral angle of 255°, these OH groups align on the same side, prompting an intramolecular H-bond interaction (H14-O13---H12-O11) that imparts stability to this particular conformer. Similarly, during the dihedral relaxed scan of C6-C4-O11-H12, a similar trend arises. At an angle of 305°, the conformer exhibits opposing orientations of the O11-H12 and S17-H18 groups. However, this arrangement shifts at an angle of 310°, causing these groups to align in the same direction and establishing an intramolecular interaction between the O11-H12 and S17-H18 moieties, thereby conferring stability to this conformer.

Across all the dihedral angle relaxed scans, the abrupt energy shifts are a direct consequence of the creation of intramolecular hydrogen bonds. This imparts additional stability to the conformers, resulting in the sharp and distinctive energy transitions observed. It is worth mentioning that the scale in figure 3.1 is set from 0° to 360° dihedral angle where angle 0° in figure 3.1(a) denotes -179.8° in the molecule. Similarly, 0° denotes 97.4° in figure 3.1(b) and 176.7° for figure 3.1(c), 177.8° in figure 3.1(d).

Population abundance help in knowing about the population of various conformers observed in the relaxed scan, therefore population abundance for DTT conformers were performed using the Boltzmann distribution equation. The results are summarized in the table 3.1 from where it is evident that the conformer G'TG'1 has the maximum cumulative population.

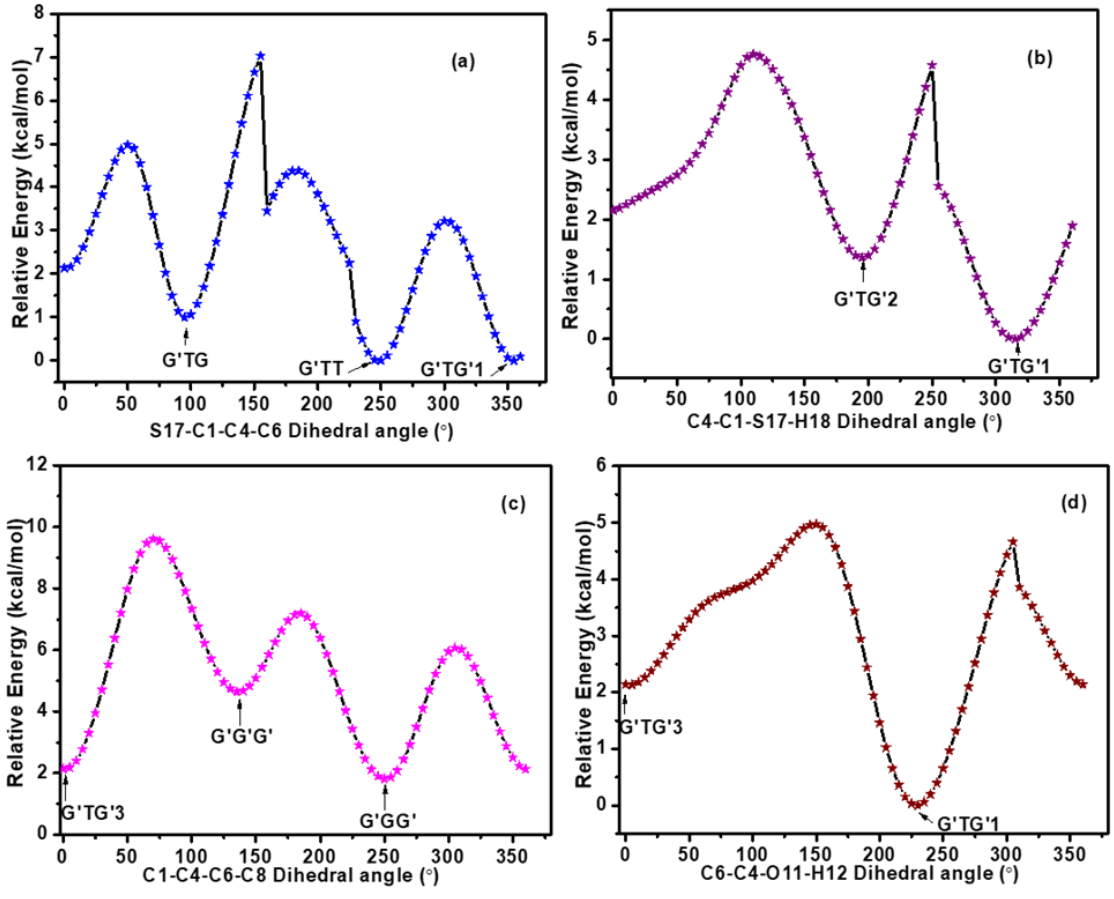

Figure 3.1: Dihedral angle-relative energy curve [with respect to G'TG'1/G'TT] (a-d) of DTT at B3LYP/cc-pVTZ level of theory

Table 3.1: Conformational abundance of the DTT conformers at B3LYP/cc-pVTZ level of theory

Dihedral angle [°]	S17-C1-C4-C6		S17-C1-C4-C6		
	ΔE [kcal/mol]	N_f [%]	Dihedral angle [°]	ΔE [kcal/mol]	N_f [%]
0	2.13	0.26	185	4.37	0.01
5	2.16	0.25	190	4.28	0.01
10	2.32	0.19	195	4.09	0.01
15	2.60	0.12	200	3.84	0.01
20	2.96	0.06	205	3.54	0.02
25	3.38	0.03	210	3.21	0.04
30	3.82	0.01	215	2.88	0.07
35	4.24	0.01	220	2.56	0.13
40	4.59	0.00	225	2.24	0.22
45	4.86	0.00	230	0.90	2.11
50	4.97	0.00	235	0.48	4.24
55	4.88	0.00	240	0.18	7.05
60	4.54	0.00	245	0.02	9.38
65	3.99	0.01	250	0.00	9.68**[G'TT]**
70	3.34	0.03	255	0.12	7.92
75	2.66	0.12	260	0.37	5.18
80	2.02	0.32	265	0.73	2.80
85	1.49	0.77	270	1.16	1.36
90	1.13	1.42	275	1.63	0.62
95	0.99	1.79**[G'TG]**	280	2.09	0.28
100	1.06	1.61	285	2.52	0.14
105	1.30	1.06	290	2.86	0.07
110	1.69	0.55	295	3.10	0.05
115	2.17	0.24	300	3.22	0.04
120	2.73	0.09	305	3.19	0.04
125	3.36	0.03	310	3.03	0.05
130	4.05	0.01	315	2.76	0.09
135	4.76	0.00	320	2.38	0.17
140	5.45	0.00	325	1.94	0.36
145	6.10	0.00	330	1.47	0.80
150	6.65	0.00	335	1.02	1.74
155	7.02	0.00	340	0.60	3.50
160	3.45	0.03	345	0.27	6.07
165	3.79	0.01	350	0.07	8.62
170	4.07	0.01	355	0.00	9.68**[G'TG'1]**
175	4.27	0.01	360	0.09	8.26
180	4.37	0.01			

These seven conformers obtained from above mentioned relaxed scans were further subjected to optimization at CCSD/cc-pVDZ level of theory to know the energy difference among them. Same energy pattern was observed among conformers at this level as well which is G'TG'1 = G'TT < G'TG <G'TG'2 < G'GG' < G'TG'3 < G'G'G'. These optimized structures, shown in figure 3.2, were found stable as they had no imaginary frequency. The relative energy difference for all seven DTT conformers was calculated with respect to most stable conformer G'TG'1/G'TT, shown in figure 3.2.

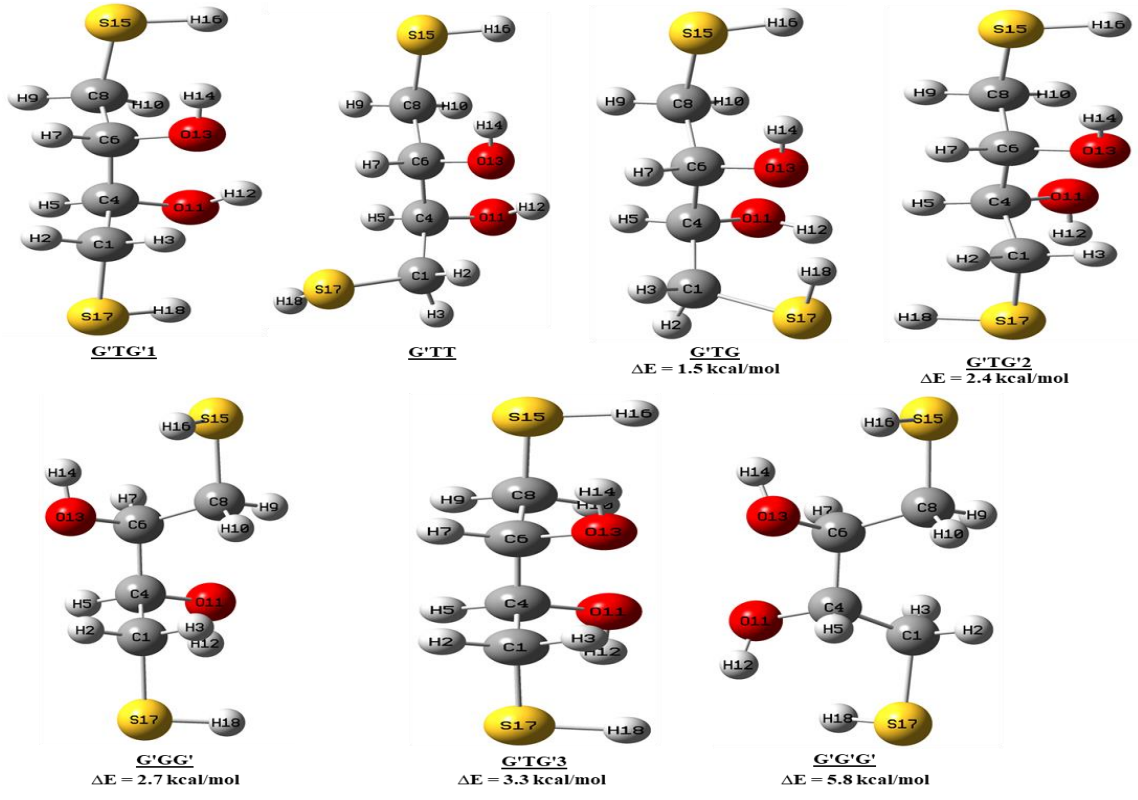

Figure 3.2: Optimized structures of all DTT conformers (numbers on atoms represent the label of that atom in the optimized geometry) where, $\Delta E = E_{conformer} - E_{GTG'1/G'TT}$

Since CCSD(T)/CBS limit level has been reported as a gold standard for energy calculation and for systems having non-covalent interactions,[24–26] single point energy was calculated for all DTT conformers at this level and the results are shown in table 3.2. The single point energies as depicted in table 3.2 follow the same energy pattern as was observed among all the DTT conformers optimized at CCSD/cc-pVDZ level of theory.

Table 3.2: Relative single point energy of all DTT conformers with respect to G'TG'1/ G'TT at CCSD(T)/CBS limit with cc-pVNZ (N=T,Q)

Conformers	CBS limit at HF,MP2, MP3, MP4, CCSD and CCSD(T) method with cc-pVNZ (N=T,Q) basis set [kcal/mol]					
	HF	MP2	MP3	MP4	CCSD	CCSD(T)
G'TG	2.02	0.85	1.08	1.04	1.13	0.90
G'TG'2	0.73	0.96	1.01	1.01	0.97	1.05
G'GG'	0.83	1.29	1.22	1.22	1.16	1.27
G'TG'3	1.45	1.88	1.83	1.83	1.79	1.86
G'G'G'	3.52	4.15	3.99	4.04	3.93	4.03

Generally, molecules with disulfide linkage have higher stability. Therefore to compare the stability of cyclic DTT (DTT that contains disulfide linkage) and acyclic DTT (does not contains disulfide linkage having only SH groups), the optimization of cyclic DTT was performed at same i.e. CCSD/cc-pVDZ level of theory. And the feasibility of cyclic to its acyclic structures (figure 3.3) was carried out by calculating their Gibbs free energy utilizing following equation:

$$E_{\text{Cyclic DTT}} + E_{H2} \rightarrow E_{\text{Acyclic DTT [G'TG'1/ G'TT]}} \qquad (1)$$

While going from its cyclic to acyclic DTT (G'TG'1/ G'TT) structure the change in Gibbs free energy was observed to be -17.52 kcal/mol indicating that the acyclic structure is more stable and dominant.

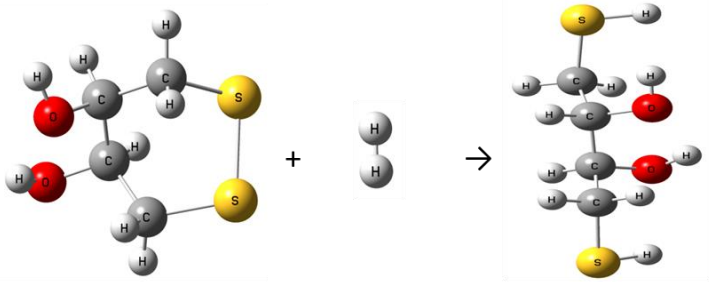

Figure 3.3: Optimized structure of Cyclic DTT, H_2 molecule and G'TG'1 at CCSD/cc-pVDZ level of theory

Furthermore, other possible configurational isomers of DTT (optimized at CCSD/cc-pVDZ level of theory) were also found to be higher in energy (figure 3.4) compared to the G'TG'1/ G'TT conformers, once again reinforcing the stability of G'TG'1/ G'TT conformers.

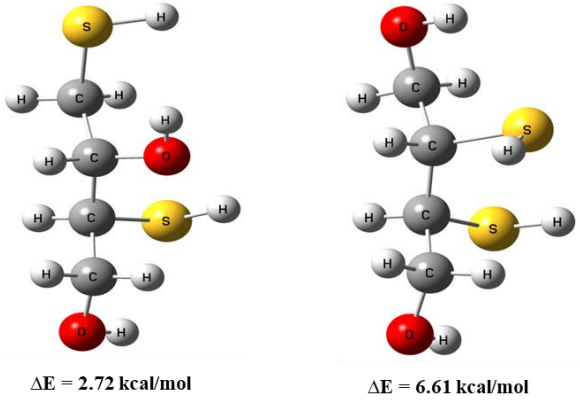

Figure 3.4: Configurational isomers of DTT molecule optimized at CCSD/cc-pVDZ level of theory; $\Delta E = E_{conformer} - E_{G'TG'1/G'TT}$

Geometrical and thermodynamic parameters of all conformers predicted at the CCSD/cc-pVDZ level of theory was found to be in good agreement with the available experimental data,[14] and the comparison is given in table 3.3, table 3.4 and table 3.5. The relative Gibbs free energy change was much lower for G'TG'1/G'TT conformers and relative enthalpy change also showed a similar pattern. The low Gibbs free energy suggests the stability of the conformer. Though, the difference was not significant in other thermodynamic parameters of all remaining DTT conformers.

Table 3.3: Optimized bond lengths in all DTT conformers and arsentite complex [As-G'TG'1/ G'TT] at CCSD/cc-pVDZ level of theory

Bond length [Å]	G'TG'1	G'TT	G'TG	G'TG'2	G'GG'	G'TG'3	G'G'G'	As-G'TG'1/ G'TT	Experimental[14]
R_{S15-C8}	1.843	1.843	1.844	1.843	1.841	1.842	1.837	1.893	1.83
R_{S17-C1}	1.834	1.835	1.839	1.838	1.841	1.842	1.837	1.884	1.83
R_{O13-C6}	1.424	1.426	1.421	1.418	1.421	1.418	1.421	1.451	1.45

R_{O11-C4}	1.422	1.421	1.413	1.415	1.421	1.418	1.421	1.409	1.43
R_{C8-C6}	1.535	1.534	1.535	1.534	1.534	1.535	1.537	1.524	1.5
R_{C6-C4}	1.538	1.537	1.539	1.535	1.536	1.534	1.534	1.51	1.53
R_{C4-C1}	1.534	1.538	1.543	1.534	1.534	1.535	1.537	1.589	1.53
R_{C8-H9}	1.104	1.104	1.104	1.105	1.102	1.105	1.104	1.1	0.64
R_{C8-H10}	1.101	1.102	1.101	1.1	1.102	1.1	1.105	1.102	0.89
R_{C6-H7}	1.11	1.107	1.112	1.112	1.109	1.112	1.109	1.102	0.76
R_{C4-H5}	1.105	1.106	1.108	1.115	1.109	1.112	1.109	1.11	0.72
R_{C1-H2}	1.105	1.104	1.104	1.104	1.102	1.105	1.104	1.101	0.93
R_{C1-H3}	1.104	1.102	1.104	1.102	1.102	1.1	1.105	1.106	0.94
$R_{O11-H12}$	0.97	0.97	0.97	0.969	0.967	0.967	0.965	0.96	0.74
$R_{H16-S15}$	1.352	1.352	1.352	1.352	1.352	1.352	1.352	-	-
$R_{H18-S17}$	1.351	1.353	1.349	1.354	1.352	1.352	1.352	-	-
$R_{H14-O13}$	0.968	0.968	0.969	0.967	0.967	0.967	0.965	-	-
R_{As-S15}	-	-	-	-	-	-	-	2.352	2.237
R_{As-S17}	-	-	-	-	-	-	-	2.373	2.247
R_{As-O13}	-	-	-	-	-	-	-	1.798	1.83

numbers after atoms represent the label of that particular atom in optimized geometry of DTT (Figure 3.2).

Table 3.4: Optimized bond angles in all DTT conformers and arsentite complex [As-G'TG'1/ G'TT] at CCSD/cc-pVDZ level of theory

Bond Angle [°]	G'TG'1	G'TT	G'TG	G'TG'2	G'GG'	G'TG'3	G'G'G'	As-G'TG'1/ G'TT	Experiment al[14]
$\theta_{S15-C8-C6}$	112.88	112.94	112.5	112.76	112.25	112.55	112.76	99.1	112.1
$\theta_{O13-C6-C8}$	111.71	111.57	111.71	111.14	112.14	111.65	110.6	104.6	108.7
$\theta_{O13-C6-C4}$	105.29	104.8	107.94	108.15	106.24	107.98	105.95	105.3	110.9
$\theta_{C8-C6-C4}$	110.72	110.76	110.89	109.91	113.05	110.96	113.15	139.6	116.3
$\theta_{O11-C4-C6}$	109.33	109.59	108.17	111.54	106.24	107.98	105.95	114.0	103.3
$\theta_{O11-C4-C1}$	111.43	109.98	111.56	112.14	112.14	111.64	110.6	111.0	109
$\theta_{C6-C4-C1}$	111.26	112.33	110.85	113.87	113.05	110.96	113.15	100.8	115.8
$\theta_{S17-C1-C4}$	112.62	114.53	112.59	115.73	112.25	112.55	112.76	119.0	114.4
$\theta_{H16-S15-C8}$	96.42	96.32	96.2	96.48	96.17	96.19	95.46	-	-
$\theta_{H14-O13-C6}$	106.23	106.2	105.65	105.54	105.96	105.63	106.53	-	-
$\theta_{H18-S17-C1}$	94.43	96.06	96.25	96.15	96.17	96.19	95.46	-	-
$\theta_{H12-O11-C4}$	104.39	104.51	105.77	105.09	105.96	105.63	106.53	-	-
$\theta_{S15-As-S17}$	-	-	-	-	-	-	-	102.3	101.2
$\theta_{S15-As-O13}$	-	-	-	-	-	-	-	84.8	89.1
$\theta_{S17-As-O13}$	-	-	-	-	-	-	-	86.0	97.1

$\Theta_{As\text{-}S15\text{-}C8}$	-	-	-	-	-	-	-	93.5	95.0
$\Theta_{As\text{-}S17\text{-}C1}$	-	-	-	-	-	-	-	99.4	99.5
$\Theta_{As\text{-}O13\text{-}C6}$	-	-	-	-	-	-	-	113.0	113.6

numbers after atoms represent the label of that particular atom in optimized geometry of DTT (Figure 3.2).

Table 3.5: Relative change in Thermodynamic parameters of all DTT conformers with respect to G'TG'1/ G'TT conformer at CCSD/cc-pVDZ level of theory

Thermodynamic Parameters (in kcal/mol)	G'TG	G'TG'2	G'GG'	G'TG'3	G'G'G'
GibbsFree Energy (ΔG)	1.35	2.06	2.12	2.56	2.5
Enthalpy(ΔH)	1.43	2.25	2.6	3.12	5.43
Entropy (ΔS)	0.0003	0.0007	0.0016	0.0019	0.0031
Heat Capacity	0.0001	0.0003	0.0006	0.0006	0.001

3.3.2 Normal modes Analysis

To get insight into its IR and Raman active vibrational modes the Experimental IR and Raman measurement was carried out for DTT powder. The observed IR and Raman active vibrational modes were then compared to the calculated vibrational modes of all DTT conformers. These calculations were performed using the B3LYP/cc-pVTZ//CCSD/cc-pVDZ level of theory. Remarkably, the calculated vibrational modes of G'TG'1 exhibited a very good agreement with the experimentally observed results. Although no peak corresponding to the G'TG'1 conformer was observed at 631 cm^{-1}, it is noteworthy that the C-S stretching peak typically falls within the 650-750 cm^{-1} range. The appearance of this peak at 631 cm^{-1} could potentially be associated with C-S stretching or bending modes, but definitive assignment remains uncertain. Also, the wave numbers observed at 2912 cm^{-1} and 2922 cm^{-1} are ascribed to the symmetric CH and CH2 stretching vibrations. It is pertinent to mention that we also identified vibrations at 2875 cm^{-1} and 2940 cm^{-1} indicative of such stretching, and the asymmetric stretching vibration of CH2 was experimentally recorded at 2975 cm^{-1}, aligning closely with the computed 2992 cm-1 frequency. (The computed CH and CH2 stretching peaks were scaled by a factor of 0.963 [27])

Notably, in IR spectrum the peaks identified at 3251 cm^{-1} and 3337 cm^{-1} can be linked to OH stretching vibrations, particularly those associated with intermolecular hydrogen bonding. Consequently, the substantial disparity between the experimental and theoretical O-H and S-H symmetric vibrational modes could potentially be attributed to the formation of intermolecular hydrogen bonding between DTT dimers during the experimental investigation.

While in the context of the experimental Raman spectrum, the peak corresponding to the OH stretching vibrational mode was not observed. This absence can be attributed to the nature of highly polar moieties, like the O-H bond, which typically exhibit weak vibrations. External electric fields are unable to induce significant alterations in the dipole moment, and the act of stretching or bending the bond does not result in considerable changes, resulting in a weak or even absent Raman signal. Figure 3.5 and 3.6 present the experimental IR and Raman spectrum of DTT, while Table 3.6 provides a detailed comparison between the experimental and calculated outcomes.

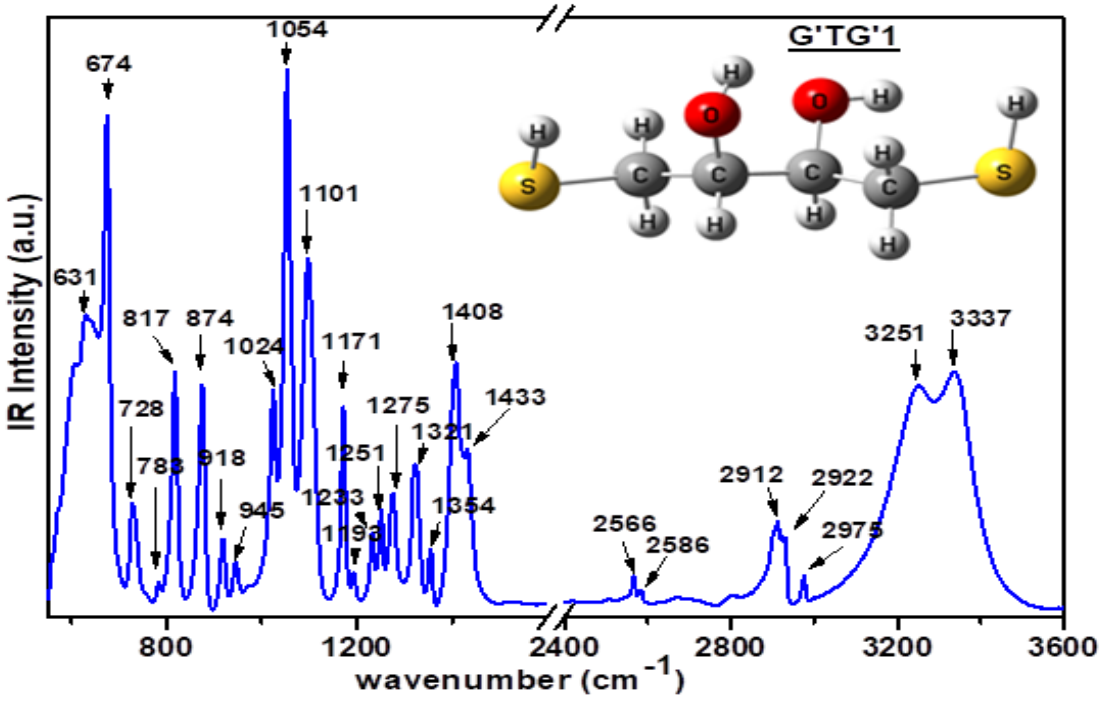

Figure 3.5: Experimental IR spectrum of DTT(solid)

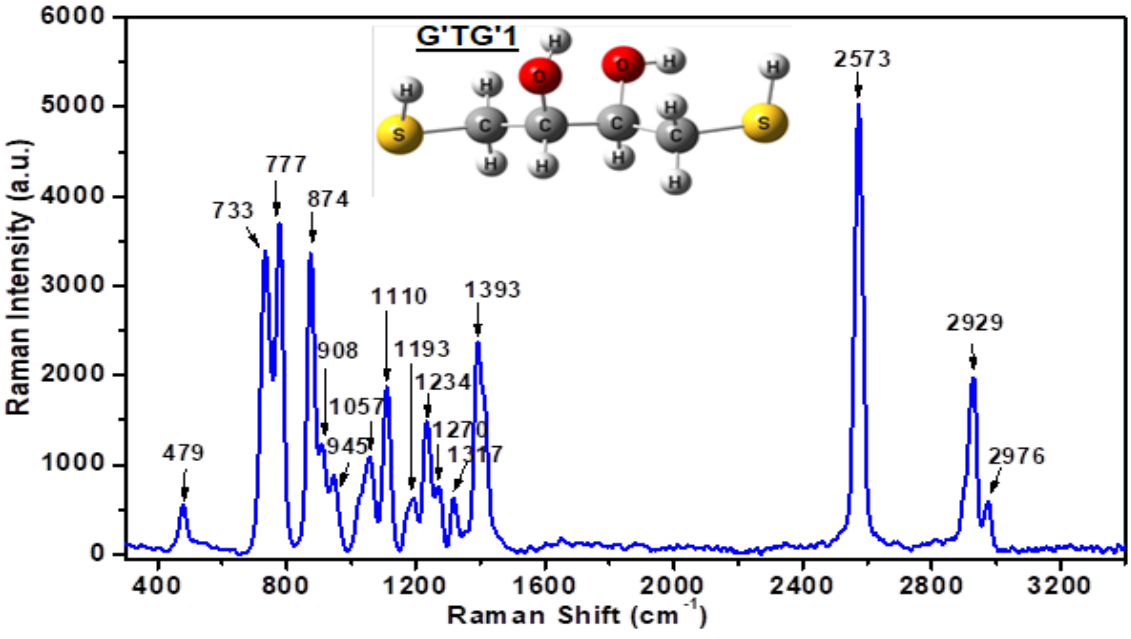

Figure 3.6: Experimental Raman spectrum of DTT(solid)

Table 3.6: Comparison of experimentally observed IR/Raman active vibrational modes with the calculated IR/Raman active modes in G'TG'1 conformer of DTT at B3LYP/cc-pVTZ//CCSD/cc-pVDZ level of theory

Experimentally observed IR active modes (cm^{-1})	**Calculated IR active modes of G'TG'1 (cm^{-1})**	**Experimentally observed Raman active modes (cm^{-1})**	**Calculated Raman active modes of G'TG'1 (cm^{-1})**	**Tentative assignment[##]**
-	-	479	463	δOH + δCCH + δSH
631	-	-	-	
674	661	-	-	νCS + δCO + δCC
728	720	733	734	νCS + δSH
783	782	777	782	δCH2 + δSH
817	809	874	877	δCH2 + δSH + δCC
918	918	908	918	δSH + δCH
945	958	945	958	δCO + δCC + δSH + δCH
1024	1034	-	-	νCC + δSH
1054	1058	1057	1058	νCO + δSH + ρCH2

1101	1113	1110	1113	νCO + δCC
1171	1176	-	-	τCH2 + δSH
1193	1205	1193	1176	τCH2 + δSH + δOH
1233	1224	1234	1224	τCH2 + δCH
1251	1260	-	-	ωCH2
1275	1278	1270	1278	ωCH2 + δCH
1321	1330	1317	1330	δOH + δCH + δCO
1354	1359	-	-	δOH + δCH
1408	1409	1393	1388	δCH + δOH + δsCH2
1433	1427	-	-	νCC + δCH + δOH + ωCH2
2566	2674	2573	2674	νSH
2586	2677	-	-	νSH
2912	2875	-	2875	νCH
2922	2940	2929	2940	νCH + ν_sCH2
2975	2992	2976	2992	νCH + ν_sCH2
3251	3737	-	3737	ν_{as}CH2
3337	3755	-	3755	νOH

ν = stretching vibration, ν_s = symmetric stretching vibration, ν_{as} = asymmetric stretching vibration, δ = bending vibration, δs = scissoring bending vibration, ρ = rocking bending vibration, τ = twisting bending vibration, ω = wagging bending vibration

3.3.3 Analysis of Intramolecular H-bond formation

The energy difference among DTT conformers is due to the difference in their structural features, particularly the possibility of intramolecular H-bonds between the OH groups and between OH and SH groups, as well as the relative orientation of these groups. It has been observed that SH groups also shows H-bonding similar to OH groups but are of weak nature comparatively.[20,22] Generally, the H-bonds are characterized by common structural features: (a) distance between the hydrogen of the donor group and the oxygen of the acceptor group, and (b) the O-H---O, O-H---S, S-H---O bond angles. The values obtained for both the above geometrical parameters (table 3.7) were found in the range usually adopted to define the H-bond.[28] The bond length between H18—O11 was calculated to be 2.48 Å in G'TG'1 conformer which is within the range between 1.89 to 2.50 Å observed in the case of threitol molecule studied by A.J. L. Jesus et al.[23] Here, S17 act as proton donor, while S15 acts as proton acceptor in the same conformer.

Besides, oxygen atom too showed strong H-bond interaction in this conformer as the bond length between H12---O13 was calculated to be 2.15 Å. These interactions are responsible for the stability of G'TG'1 conformer. Similarly, these interactions though slightly weak were observed in other conformers of DTT on the basis of H-Bond length between H atom and electronegative atoms (S and O).

Table 3.7: Hydrogen-bond parameters for all DTT conformers at CCSD/cc-pVDZ level

H-Bond length [Å]	G'TG'1	G'TT	G'TG	G'TG'2	G'GG'	G'TG'3	G'G'G'
S17-H18---O11	**2.48**	4.21	3.44	3.56	2.94	3.02	**2.7**
O11-H12---O13	**2.15**	**2.14**	**2.58**	3.63	4.27	3.71	3.43
O13-H14---S15	**2.59**	**2.61**	**2.55**	**2.66**	**2.73**	**2.66**	2.87
O11-H12---S17	3.64	4.4	**2.58**	**2.55**	**2.73**	**2.66**	2.87
Bond Angle [°]	G'TG'1	G'TT	G'TG	G'TG'2	G'GG'	G'TG'3	G'G'G'
S17-H18---O11	**107.8**	75.2	65.3	61.2	86.7	82.6	**94.3**
O11-H12---O13	**113.4**	**113.6**	**95.6**	32.3	40	22.6	42.3
O13-H14---S15	**114.8**	**112.9**	**116.3**	**111.5**	**107.7**	**111.3**	95.2
O11-H12---S17	53.7	65	**115.8**	**119.2**	**107.7**	**111.3**	95.2

Note: numbers in bold are in the range usually adopted to define the H-bond, therefore suggesting the possibility of intramolecular H-bond formation.

AIM calculations based on electron density calculation $\rho(r)$ and Laplacian electron density $\nabla^2\rho(r)$ calculations have been found very helpful in furthering deeper insights about non-covalent interactions, notwithstanding its limitations.[29–31] Therefore, to know the number and types of intramolecular H-bond interactions present in DTT molecule and to assess their binding energy, AIM calculations were carried out for all the conformers (shown in figure 3.7 and table 3.8) which revealed the presence of intramolecular H-bond interactions in only four of the conformers (G'TT, G'TG, G'TG'2 and G'GG').

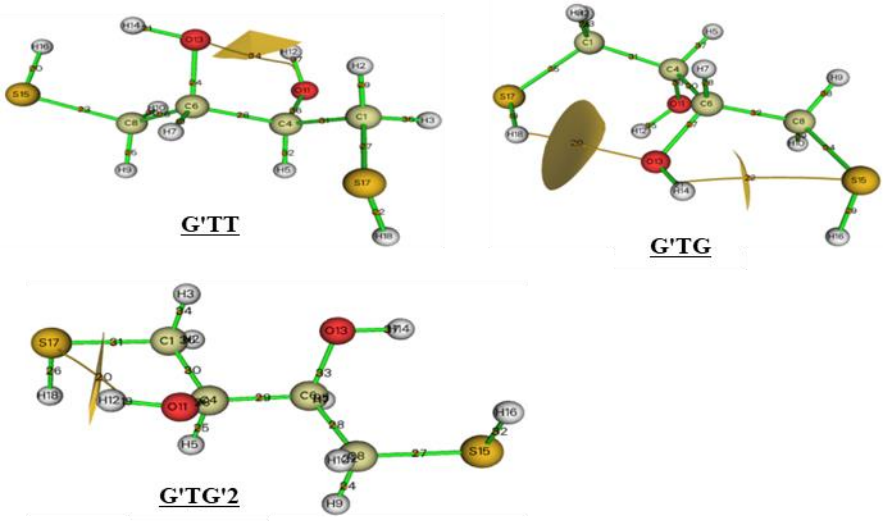

Figure 3.7: Topological basin surfaces with Bond critical points (3,-1) of DTT at CCSD/cc-pVDZ level

Table 3.8: Topological parameters for bonds of interacting atoms in DTT: electron density (ρBCP), kinetic electron energy density (GBCP), potential electron energy density (VBCP), total electron energy density (HBCP), Laplacian of electron density (∇^2 BCP), estimated interaction energy (E_{int}) at bond critical point (BCP)

G'TT						
Critical Point number	**ρBCP [a.u.]**	**G_{BCP} [a.u.]**	**V_{BCP} [a.u.]**	**H_{BCP} [a.u.]**	**∇^2ρBCP [a.u.]**	**E_{int} [kcal/mol]**
34[O13---H12]	0.01993	0.02105	-0.01988	0.00117	0.08888	-3.70
G'TG						
20[O13---H18]	0.01553	0.01236	-0.01230	0.00006	0.04968	-3.86
22[S15---H14]	0.01575	0.01322	-0.01210	0.00112	0.05736	-3.80
G'TG'2						
20[S17---H12]	0.01599	0.01310	-0.01206	0.001035	0.05655	-3.78

From the topological analysis of BCP weak intramolecular H-bonds were observed in DTT conformers. To know the strength of H-bond 3 conditions were set by

Rozas et al.[32] these are: if Laplacian electron density $\nabla^2\rho < 0$ and $H < 0$, H- bond is strong and of covalent nature and when $\nabla^2\rho > 0$ and $H < 0$, H-bond is of medium strength and partially covalent and $\nabla^2\rho > 0$ and $H > 0$ represents the weak nature of H-bond. As shown in table, G'TT, G'TG and G'TG'2 were found to have intramolecular H-bond interactions. The equation formulated by Emamian et al.[33] was utilized to calculate hydrogen bond energies. All these interactions show reasonably good interaction energies. Thus it is inferred that in DTT, along with Oxygen atom Sulfur atom also shows intramolecular H-bonding.

Furthermore, RDG analysis of DTT conformers was carried out in order to differentiate and visualize various kinds of non-covalent interactions in DTT. The theory of RDG calculation is already explained in the introduction section 1.6.5.

In order to have a clear depiction of different types of interactions the color gradient was used which stand for ρ (r) and $\lambda 2$ value, and filled in the RDG iso-surfaces as shown in figure 3.8(b). The contour value was set to 0.5 (shown in figure 3.8(a). These results were calculated and visualized by Multiwfn and VMD software. In figure 3.8(b), the interaction regions marked in blue correspond to H-bond interactions while those marked in green to Van der Waals interaction and red to repulsive interactions. Whereas the scatter plot and RDG iso-surface for conformer G'TG'1/G'TT are shown in the figure herein, for other conformers it is provided in supplementary information. Intramolecular H-bond interaction between O-H---O, S-H---O and O-H---S in G'TG'1/G'TT conformers gets evident from figure 3.8b which contribute towards the stability of these conformers. Weak Van der Waals interactions in other conformers of DTT were also observed as shown in figure 3.8(b).

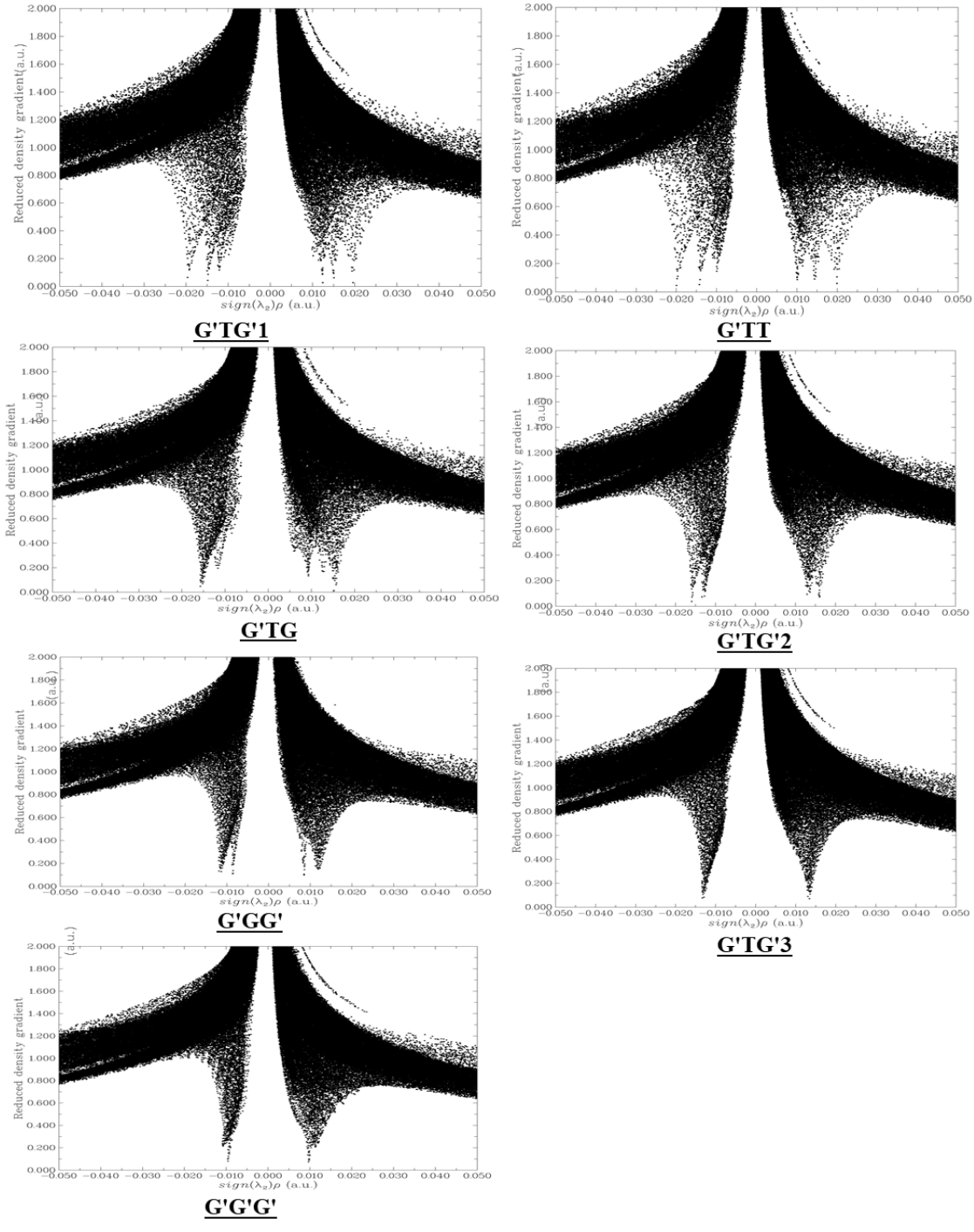

Figure 3.8(a): Scatter plot of the reduced density gradient (RDG(r)) versus Ω(r) for all seven conformers of DTT [where, iso-surface of RDG = 0.5]

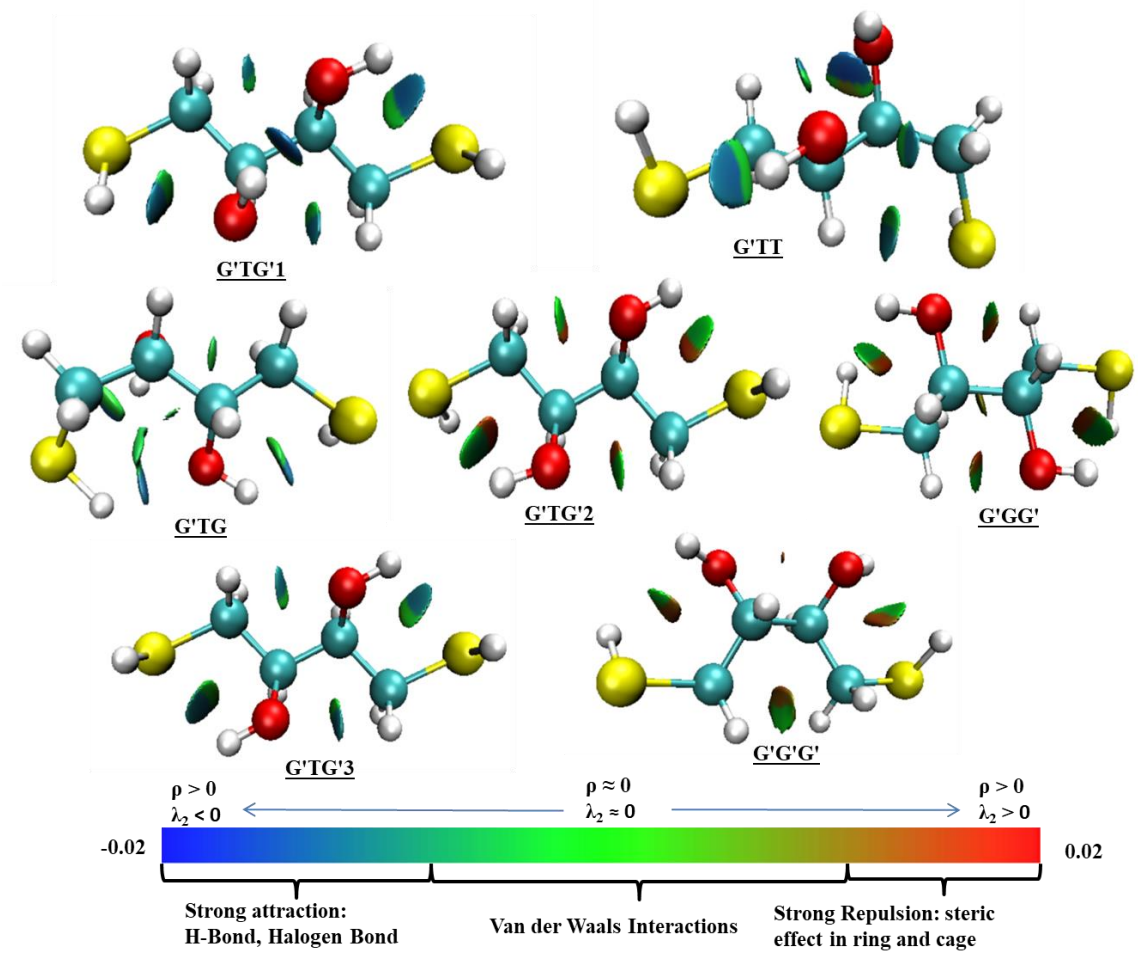

Figure 3.8(b): The visual diagram of RDG iso-surfaces for DTT conformers. Color gradient corresponds to the different types of interaction in respective conformers

3.3.4 NBO calculations

Although the AIM and NCI analysis revealed the possibility of intramolecular H-bond interactions, other possible hyperconjugative interactions, to have insight into exact orbitals involved in and extent of charge-transfer the NBO calculations was performed. From NBO analysis it was observed that in G'TG'1, there is hyperconjugative interaction between C1-H2---S17-H18 bonds. Also, the bond pair of C4-H5 bond is donated to antibonding orbital σ*(O11-H12). Besides, the O11 lone-pair is donated to σ*(C1-C4), σ*(C4-C6) antibonding orbitals. And a very feeble electron density transfers to the σ*(S17-H18) antibonding orbital. Whereas, O13 lone-pair is donated to σ*(O11-H12)

orbital suggesting the formation of intramolecular H-bond but also shows very strong hyperconjugative interaction with the σ*(C6-C7) and σ*(C6-C8) orbitals. While in the case of S15 its lone-pair has hyperconjugative interaction with σ*(C6-C8) [strong] and with σ*(C8-H10), σ*(C8-H9) [weak] orbitals. Besides, a very weak intramolecular H-bond was also formed between n(S15) → σ*(O13-H14). However, the S17 lone-pair showed only hyperconjugative interactions: n(S17) → σ*(C1-H3), n(S17) → σ*(C1-H4) sans any other intramolecular H-bond interactions (n denotes non-bonded electrons).

Intramolecular H-bond formation between O13 atom and H12 atom of H12-O11 bond orbital [n(O13) →σ*(H12-O11)] was observed in the G'TT conformer. And the other comparatively strong n(S15) → σ*(H14-O13) H-bond formation was also observed. Many other hyperconjugative interactions similar to G'TG'1 conformer were observed. While in conformer G'TG, there was in place of n(O13) → σ*(H12-O11), quite a strong n(S17) → σ*(H12-O11) and a weak n(O13) → σ*(H18-S17) intramolecular H-bond formation. Other intramolecular interactions were found to be similar to G'TT conformer. Whereas, in G'TG'2, G'GG', G'TG'3 and G'G'G' conformers, very weak intramolecular H-bond interactions n(S15) → σ*(H14-O13) and n(S17) → σ*(H12-O11) were observed along with the other stabilized hyperconjugative interactions as n(O11) → σ*(C4-H3), n(O13) → σ*(C6-H7), n(S15) → σ*(C6-C8). These interactions overall provide stability to DTT molecule. Some significant donor-acceptor NBO interactions are shown in table 3.9.

Table 3.9: Some significant donor - acceptor NBO interactions in DTT molecule with calculated second order stabilization energies E(2) kcal/mol

Donor→ Acceptor	E(2) [kcal/mol]						
	G'TG'1	G'TT	G'TG	G'TG'2	G'GG'	G'TG'3	G'G'G'
σC1-H2→ σ*S17-H18	1.75	1.88	1.97	-	1.56	1.38	1.74
σC1-H3→ σ*S17-H18	-	-	-	1.97	-	-	-
σC1-H2→ σ*C4-O11	-	-	-	5.95	6.53	6.32	5.70
σC4-H5→ σ*C6-O13	-	-	-	5.86	-	5.88	1.57
σC4-H5→ σ*O11-H12	3.80	3.80	4.21	-	-	-	-
σC4-C6→ σ*O11-H12	-	-	-	2.76	2.89	2.76	2.34
σC4-C6→ σ*O13-H14	-	-	-	2.77	2.89	2.76	2.34

σC8-H9→ σ*S15-H16	-	-	-	-	1.56	1.38	1.74
LPO11→ σ*C1-C4	8.87	9.73	6.57	5.67	9.11	8.54	10.16
LPO11→ σ*C4-C6	5.28	4.30	9.54	1.09	-	1.05	1.40
LPO11→ σ*C4-H5	-	-	-	11.30	6.73	7.79	3.71
LPO11→ σ*S17-H18	1.08	-	-	-	-	-	-
LPO13→ σ*S17-H18	-	-	1.50	-	-	-	-
LPO13→ σ*O11-H12	1.51	1.77	-	-	-	-	-
LPO13→ σ*C6-H7	9.93	8.59	7.85	7.96	6.73	7.79	3.72
LPO13→ σ*C6-C8	5.62	6.56	7.91	8.45	9.11	8.54	10.16
LPS15→ σ*C8-H10	1.78	1.76	1.76	1.66	2.35	1.74	3.83
LPS15→ σ*C6-C8	5.99	6.01	5.90	6.03	5.61	6.05	5.60
LPS15→ σ*C8-H9	1.71	1.48	1.88	1.31	-	1.26	-
LPS15→ σ*O13-H14	2.87	2.48	3.35	**1.96**	**1.32**	**1.93**	**0.52**
LPS17→ σ*C1-H3	6.37	4.00	5.17	-	2.35	1.74	3.83
LPS17→ σ*C1-H2	-	-	-	5.02	-	1.26	-
LPS17→ σ*C1-C4	3.68	6.09	5.62	4.53	5.91	6.05	5.60
LPS17→ σ*C4-O11	-	1.47	-	-	-	-	-
LPS17→ σ*O11-H12	-	-	3.14	**3.81**	**1.32**	**1.93**	**0.52**

LP denotes lone pair of electrons, σ denotes sigma bonding orbital, σ* denotes sigma antibonding orbital and numbers after atoms represent the label of respective atom (figure 3.2).

3.3.5 ESP Charge and FMO Analysis

To analyze the impact of intramolecular charge transfers on the atomic charges of DTT, ESP[MK(Merz Kollman)] charge calculations were conducted at the CCSD/cc-pVDZ level of theory. Figure 3.9 illustrates the charge distribution plot obtained from ESP[MK] calculation. These ESP results provide further support to the previously discussed AIM and NBO findings. The atomic charges for all DTT conformers can be found in the table 3.10. Additionally, Hirshfeld charge calculations were performed for all conformers, revealing a similar charge pattern to that of ESP[MK] charges. The charge distribution curve for Hirshfeld charges and the corresponding atomic charge values are presented in table 3.11 and figure 3.10 respectively. Also, to identify the regions of positive and negative electrostatic potential within the molecule, ESP mapping was performed on the optimized structures of all DTT conformers. The resulting maps, showcasing the distribution of charged electrostatic potential, is shown in figure 3.11.

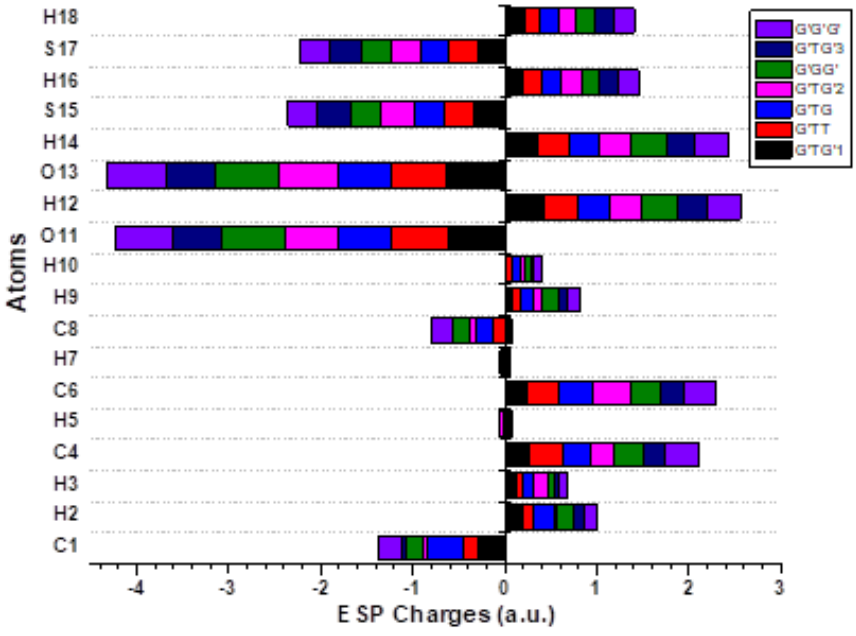

Figure 3.9: Charge distribution plot of ESP[MK] charges for DTT conformers; the number after atoms represent the label of that atom shown in figure 3.2

Table 3.10: The ESP[MK] charge values [a.u.] on each atom of DTT conformers at CCSD/cc-pVDZ level of theory

ESP Charge Values (a.u.)							
Atoms	G'TG'1	G'TT	G'TG	G'TG'2	G'GG'	G'TG'3	G'G'G'
C1	-0.293	-0.164	-0.377	-0.046	-0.192	-0.040	-0.253
H2	0.183	0.132	0.229	0.012	0.196	0.101	0.145
H3	0.122	0.081	0.099	0.161	0.084	0.041	0.090
C4	0.259	0.381	0.303	0.243	0.325	0.234	0.367
H5	0.027	-0.007	-0.004	-0.042	0.017	0.001	0.028
C6	0.232	0.350	0.378	0.410	0.322	0.252	0.354
H7	0.007	-0.018	0.009	-0.022	0.018	-0.009	0.025
C8	0.050	-0.133	-0.180	-0.062	-0.178	0.021	-0.241
H9	0.077	0.098	0.125	0.096	0.193	0.079	0.154
H10	0.014	0.064	0.084	0.053	0.077	0.023	0.086
O11	-0.602	-0.627	-0.575	-0.575	-0.692	-0.527	-0.637
H12	0.423	0.365	0.358	0.347	0.392	0.312	0.364
O13	-0.627	-0.603	-0.578	-0.643	-0.692	-0.539	-0.641
H14	0.363	0.339	0.319	0.338	0.392	0.317	0.369
S15	-0.345	-0.311	-0.327	-0.359	-0.336	-0.352	-0.322

H16	0.201	0.196	0.211	0.221	0.202	0.211	0.213
S17	-0.299	-0.321	-0.280	-0.324	-0.333	-0.341	-0.317
H18	0.207	0.178	0.204	0.190	0.201	0.213	0.212

numbers represent label of that atom (figure 3.2).

Table 3.11: The Hirshefield charge values [a.u.] on each atom of DTT conformers at CCSD/cc-pVDZ level of theory

Hirshfeld Charge Values (a.u.)							
Atoms	G'TG'1	G'TT	G'TG	G'TG'2	G'GG'	G'TG'3	G'G'G'
C1	-0.033	-0.030	-0.027	-0.027	-0.030	-0.028	-0.031
H2	0.032	0.034	0.035	0.032	0.039	0.033	0.033
H3	0.028	0.033	0.029	0.040	0.030	0.038	0.030
C4	0.077	0.077	0.079	0.076	0.075	0.075	0.075
H5	0.029	0.026	0.031	0.013	0.023	0.017	0.025
C6	0.072	0.066	0.069	0.075	0.075	0.075	0.075
H7	0.023	0.016	0.017	0.016	0.023	0.017	0.025
C8	-0.027	-0.028	-0.028	-0.027	-0.030	-0.028	-0.031
H9	0.036	0.036	0.034	0.033	0.039	0.033	0.033
H10	0.038	0.036	0.038	0.039	0.030	0.038	0.030
O11	-0.260	-0.265	-0.264	-0.260	-0.262	-0.259	-0.261
H12	0.151	0.151	0.140	0.138	0.149	0.145	0.156
O13	-0.256	-0.257	-0.256	-0.259	-0.262	-0.259	-0.261
H14	0.145	0.146	0.140	0.145	0.149	0.145	0.156
S15	-0.061	-0.064	-0.063	-0.072	-0.072	-0.072	-0.075
H16	0.049	0.047	0.049	0.048	0.044	0.048	0.047
S17	-0.091	-0.069	-0.072	-0.057	-0.072	-0.072	-0.075
H18	0.046	0.042	0.044	0.042	0.045	0.048	0.047

numbers represent label of that atom (figure 3.2).

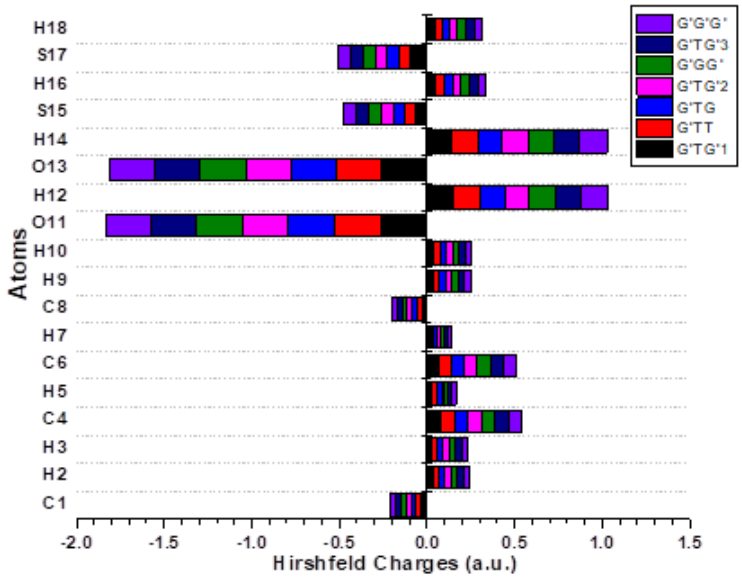

Figure 3.10: Charge distribution plot of Hirshfeld charges for all DTT conformers at CCSD/cc-pVDZ level of theory

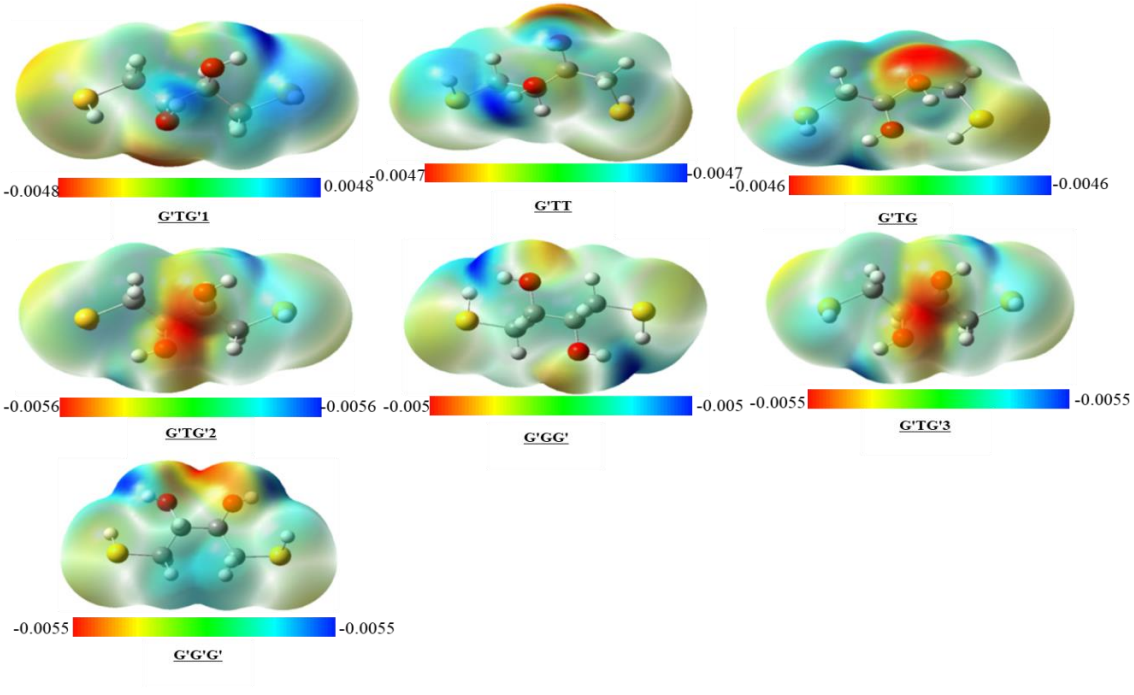

Figure 3.11 : ESP map on optimized geometries of DTT conformers at CCSD/cc-pVDZ level

From the ESP maps it was observed that the negative potential was located over oxygen atoms in all conformers rendering it prone to electrophilic attack while the positive electrostatic potential was located on oxygenated proton atoms in all the conformers rendering it as an attractive center for nucleophilic attack.

FMO calculations were conducted at the CCSD/cc-pVDZ level of theory for all conformers. Among them, the G'TG'1 conformer (global minimum) exhibited the lowest gap between its HOMO and LUMO (H-L), measuring 13.30 eV. The remaining conformers displayed slightly higher H-L gaps compared to the global minimum. The significantly lower H-L gap of the G'TG'1 conformer suggests its comparatively higher reactivity. The frontier molecular orbitals are depicted in figure 3.12, while the calculated energy parameters of FMOs for DTT conformers are presented in table 3.12.

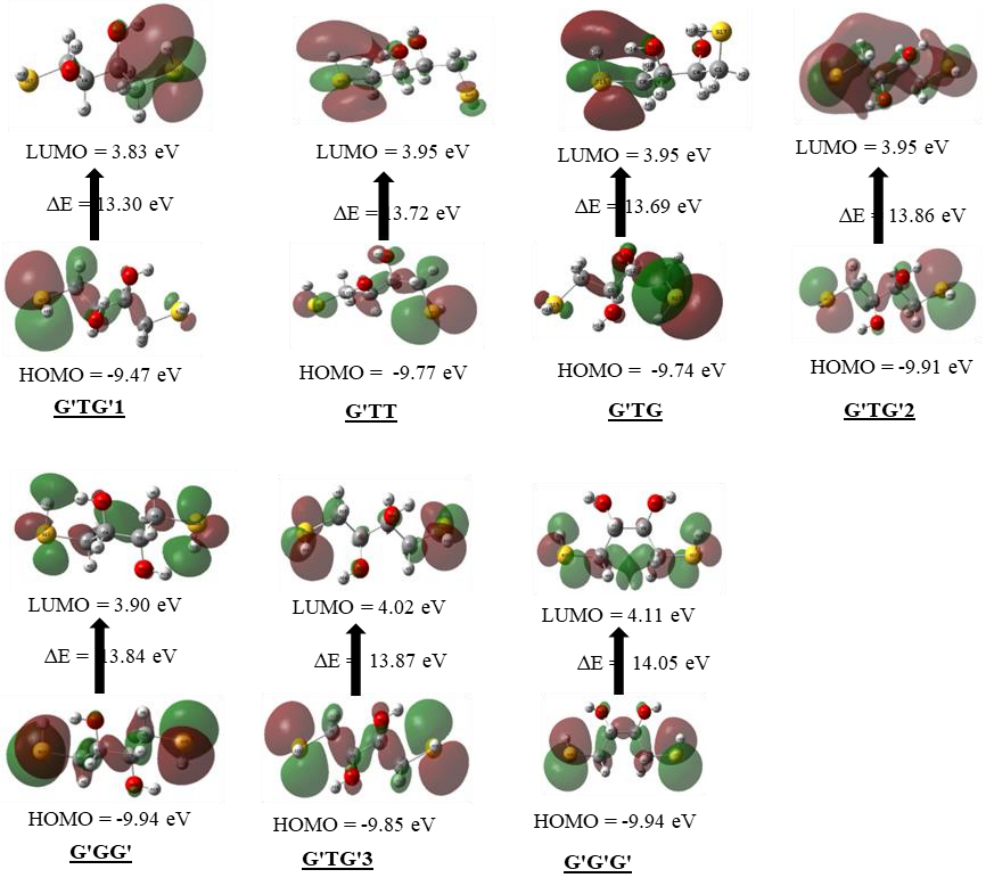

Figure 3.12: HOMO-LUMO (ΔE) gap of all DTT conformers at CCSD/cc-pVDZ

Table 3.12: Computed energy [eV] parameters of all DTT conformers at CCSD/cc-PVDZ level of theory

Energy Parameters	G'TG'1	G'TT	G'TG	G'TG'2	G'GG'	G'TG'3	G'G'G'
E_{HOMO} (IP) [eV]	-9.47	-9.77	-9.75	-9.91	-9.94	-9.85	-9.94
E_{LUMO} (EA) [eV]	3.83	3.95	3.95	3.95	3.90	4.02	4.11
HOMO-LUMO gap [eV]	13.30	13.72	13.69	13.86	13.84	13.87	14.05
Dipole moment [D]	2.50	0.83	1.84	1.76	0.23	0.40	0.13
Hardness(η) [eV]	-2.82	-2.91	-2.90	-2.98	-3.02	-2.92	-2.92
Chemical potential(μ) [eV]	-6.65	-6.86	-6.85	-6.93	-6.92	-6.94	-7.03
Electronegativity(χ) [eV]	-2.82	-2.91	-2.90	-2.98	-3.02	-2.92	-2.92
Electrophilicity index(ω) [eV]	-7.84	-8.08	-8.09	-8.05	-7.92	-8.25	-8.46

It was observed that in all the conformers of DTT the HOMO and LUMO is located majorly over sulfur and oxygen atoms of this molecule. G'TG'1 showed highest dipole moment among all conformers which further indicates a substantial charge arrangement in this conformer differing from the rest. Similarly, the low value of hardness for G'TG'1 conformer further suggests its increased reactivity. Values of other parameters like μ, ω and χ support the above prediction.

UV-visible spectrum of DTT (G'TG'1/G'TT) computed at TD-DFT level revealed peaks at 196.8 nm (λmax) (oscillator strength = 0.0096), 216.8 nm (oscillator strength = 0.0016) and 217.8 nm (oscillator strength = 0.001), respectively (shown in figure 3.13), which substantiated the experimental observation[34] where the λ_{max} of reduced DTT was below 260 nm. For the calculation of UV-visible spectrum, the optimized geometry of G'TG'1 conformer at CCSD/cc-pVDZ level used and further re-optimized at B3LYP/cc-pVTZ level using TD-DFT method in methanol solvent utilizing implicit solvation model.[35]

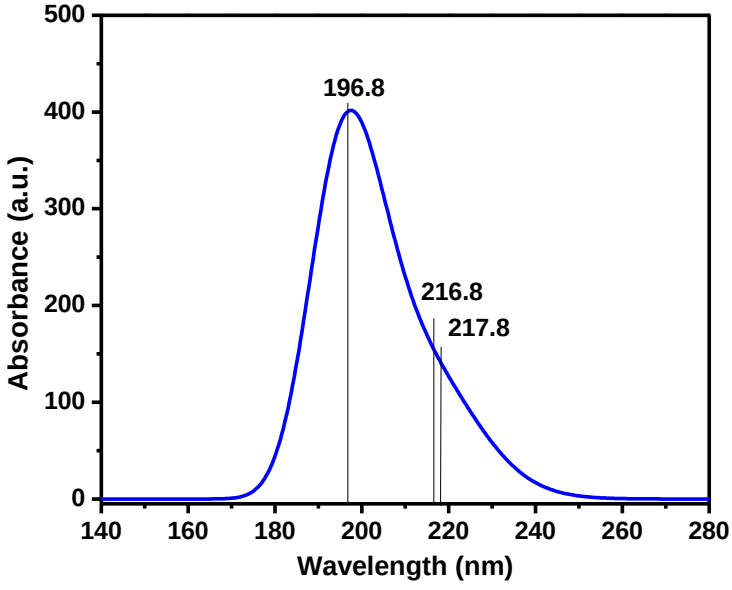

Figure 3.13: Calculated UV spectrum of G'TG'1/G'TT conformer (λmax = 196.8 nm) of DTT

^{1}H NMR spectrum was calculated using GIAO method and the peaks were in good agreement with the literature.[36,37] In the experiment ^{1}H NMR peaks were observed in $CDCl_3$ while in the simulated ^{1}H NMR the methanol solution with TMS was utilized at B3LYP/cc-pVTZ//CCSD/cc-pVDZ level of theory. Experimentally observed and simulated ^{1}H NMR peaks are compared in table 3.13. Despite the fact that G'TG'1 and G'TT conformers are both iso-energic, their structural differences are apparent as evidenced by the predicted NMR peaks. The distinction in the H18 peak between these conformers can be attributed to the deshielding of the H18 proton in the G'TG'1 conformer. This deshielding results from the formation of an H-bond between S17-H18 and O11, a characteristic not present in the G'TT conformer.

Table 3.13: Comparison of experimental and simulated ^{1}H NMR peaks of DTT Conformer (G'TG'1/G'TT)

^{1}H NMR peaks [ppm]			Assignment[#]
Reported in literature[36,37] [in $CDCl_3$] with TSP, δ	Simulated peaks, δ [in CH_3OH with TMS]		
	G'TG'1	G'TT	
3.6-3.7	3.7	3.4	H5, m
3.3	3.0	1.9	H18, s
2.5-2.9	3.6	3.1	H3, m
2.5-2.9	2.8	2.6	H2, m

[#]: s and m denote multiplicity of the peaks namely singlet and multiplet respectively, number after atoms represent the label of the proton atom shown in figure 3.2.

3.4 Conclusion

The conformational space of DTT has several local minima and among them, the lowest iso-energic conformers were identified as G'TG'1 and G'TT. Analysis of AIM and NCI calculations revealed that there is intra-molecular H-bond formation not only by OH groups but by SH groups as well which provides stability to the titled molecule. NBO results, besides reiterating these intramolecular H-bond interactions, revealed other hyperconjugative interactions which further imparts the stability to DTT molecule. ESP charge analysis supports these observations very well. The calculated vibrational spectra too were found in good agreement with the observed experimental data.

3.5 References

(1) Cleland, W. W. Dithiothreitol, a New Protective Reagent for SH Groups. *Biochemistry* **1964**, *3* (4), 480–482.

(2) Klonne, D. R.; Johnson, D. R. Enzyme Activity and Sulfhydryl Status in Rat Renal Cortex Following Mercuric Chloride and Dithiothreitol Administration. *Toxicol. Lett.* **1988**, *42* (2), 199–205.

(3) Reynolds, I. J.; Rush, E. A.; Aizenman, E. Reduction of NMDA Receptors with Dithiothreitol Increases [3H]-MK-801 Binding and NMDA-Induced Ca2+ Fluxes. *Br. J. Pharmacol.* **1990**, *101* (1), 178–182.

(4) Aizenman, E.; Lipton, S. A.; Loring, R. H. Selective Modulation of NMDA Responses by Reduction and Oxidation. *Neuron* **1989**, *2* (3), 1257–1263.

(5) Sakai, T.; Yanagihara, S.; Kunugi, Y.; Ushio, K. Mechanisms of ALA-D Inhibition by Lead and of Its Restoration by Zinc and Dithiothreitol. *Occup. Environ. Med.* **1983**, *40* (1), 61–66.

(6) Zhang, R.; Snyder, G. H. Kinetics of Disulfide Exchange Reactions of Monomer and Dimer Loops of Cysteine-Valine-Cysteine Peptides. *Biochemistry* **1988**, *27* (10), 3785–3794.

(7) Bick, Y.; Jackson, W. Chemical Protection against X-Irradiation by a New Reducing Agent 1, 4-Dithiothreitol in Marsupial Leucocytes in Culture. *Nature* **1968**, *217* (5127), 479–480.

(8) Gailis, L. Cleland's Reagents Block Lethal and Hypnotic Effects of Pentobarbital. *Eur. J. Pharmacol. Environ. Toxicol. Pharmacol.* **1994**, *292* (1), 39–42.

(9) Nicolas, J.; Jaafar, M.; Sepetdjian, E.; Saad, W.; Sioutas, C.; Shihadeh, A.; Saliba, N. A. Redox Activity and Chemical Interactions of Metal Oxide Nano-and Micro-Particles with Dithiothreitol (DTT). *Environ. Sci. Process. Impacts* **2015**, *17* (11), 1952–1958.

(10) Ismail, T.; Qureshi, M.; Akhtar, N.; Mansoor, Q.; Ismail, M. Synthesis, Characterization and DNA Cleavage of Copper (II) Complex with D, L-Dithiothreitol. *Trop. J. Pharm. Res.* **2016**, *15* (3), 599–603.

(11) Becker, O. M.; MacKerell Jr, A. D.; Roux, B.; Watanabe, M. *Computational Biochemistry and Biophysics*; Crc Press, 2001.

(12) Mavromoustakos, T.; Zervou, M.; Zoumpoulakis, P.; Kyrikou, I.; Benetis, N.; Polevaya, L.; Roumelioti, P.; Giatas, N.; Zoga, A.; Minakakis, P. M. Conformation and Bioactivity. Design and Discovery of Novel Antihypertensive Drugs. *Curr. Top. Med. Chem.* **2004**, *4* (4), 385–401.

(13) Masnabadi, N.; Thalji, M. R.; Alhasan, H. S.; Mahmoodi, Z.; Soldatov, A. V.; Ali, G. A. Structural, Electronic, Reactivity, and Conformational Features of 2, 5, 5-Trimethyl-1, 3, 2-Diheterophosphinane-2-Sulfide, and Its Derivatives: DFT, MEP, and NBO Calculations. *Molecules* **2022**, *27* (13), 4011.

(14) Cruse, W.; James, M. The Crystal Structure of the Arsenite Complex of Dithiothreitol. *Acta Crystallogr. B* **1972**, *28* (5), 1325–1331.

(15) Perlstein, J. The Weak Hydrogen Bond In Structural Chemistry and Biology (International Union of Crystallography, Monographs on Crystallography, 9) By Gautam R. Desiraju (University of Hyderabad) and Thomas Steiner (Freie Universität Berlin). Oxford University Press: Oxford and New York. 1999. Xiv+ 507 Pp. $150. ISBN 0-19-850252-4., 2001.

(16) Desiraju, G. R.; Steiner, T. *The Weak Hydrogen Bond: In Structural Chemistry and Biology*; International Union of Crystal, 2001; Vol. 9.

(17) Zhou, P.; Tian, F.; Lv, F.; Shang, Z. Geometric Characteristics of Hydrogen Bonds Involving Sulfur Atoms in Proteins. *Proteins Struct. Funct. Bioinforma.* **2009**, *76* (1), 151–163.

(18) Biswal, H. S.; Bhattacharyya, S.; Bhattacherjee, A.; Wategaonkar, S. Nature and Strength of Sulfur-Centred Hydrogen Bonds: Laser Spectroscopic Investigations in the Gas Phase and Quantum-Chemical Calculations. *Int. Rev. Phys. Chem.* **2015**, *34* (1), 99–160.

(19) Chand, A.; Sahoo, D. K.; Rana, A.; Jena, S.; Biswal, H. S. The Prodigious Hydrogen Bonds with Sulfur and Selenium in Molecular Assemblies, Structural Biology, and Functional Materials. *Acc. Chem. Res.* **2020**, *53* (8), 1580–1592.

(20) Arunan, E.; Emilsson, T.; Gutowsky, H.; Fraser, G. T.; De Oliveira, G.; Dykstra, C. Rotational Spectrum of the Weakly Bonded C 6 H 6–H 2 S Dimer and Comparisons to C 6 H 6–H 2 O Dimer. *J. Chem. Phys.* **2002**, *117* (21), 9766–9776.

(21) Goswami, M.; Arunan, E. Microwave Spectrum and Structure of C6H5CCH⋯ H2S Complex. *J. Mol. Spectrosc.* **2011**, *268* (1–2), 147–156.

(22) Lobo, I. A.; Robertson, P. A.; Villani, L.; Wilson, D. J.; Robertson, E. G. Thiols as Hydrogen Bond Acceptors and Donors: Spectroscopy of 2-Phenylethanethiol Complexes. *J. Phys. Chem. A* **2018**, *122* (36), 7171–7180.

(23) Jesus, A. J. L.; Tomé, L. I.; Rosado, M. T. S.; Leitão, M. L. P.; Redinha, J. S. Conformational Study of Erythritol and Threitol in the Gas State by Density Functional Theory Calculations. *Carbohydr. Res.* **2005**, *340* (2), 283–291.

(24) Rezac, J.; Simova, L.; Hobza, P. CCSD [T] Describes Noncovalent Interactions Better than the CCSD (T), CCSD (TQ), and CCSDT Methods. *J. Chem. Theory Comput.* **2013**, *9* (1), 364–369.

(25) Rezac, J.; Hobza, P. Describing Noncovalent Interactions beyond the Common Approximations: How Accurate Is the "Gold Standard," CCSD (T) at the Complete Basis Set Limit? *J. Chem. Theory Comput.* **2013**, *9* (5), 2151–2155.

(26) Ramabhadran, R. O.; Raghavachari, K. Extrapolation to the Gold-Standard in Quantum Chemistry: Computationally Efficient and Accurate CCSD (T) Energies for Large Molecules Using an Automated Thermochemical Hierarchy. *J. Chem. Theory Comput.* **2013**, *9* (9), 3986–3994.

(27) Jesus, A. L.; Redinha, J. On the Structure of Erythritol and L-Threitol in the Solid State: An Infrared Spectroscopic Study. *J. Mol. Struct.* **2009**, *938* (1–3), 156–164.

(28) Steiner, T. The Hydrogen Bond in the Solid State. *Angew. Chem. Int. Ed.* **2002**, *41* (1), 48–76.

(29) Matta, C. F.; Boyd, R. J. An Introduction to the Quantum Theory of Atoms in Molecules. *Quantum Theory At. Mol. Solid State DNA Drug Des.* **2007**.

(30) Waller, M. P.; Robertazzi, A.; Platts, J. A.; Hibbs, D. E.; Williams, P. A. Hybrid Density Functional Theory for π-Stacking Interactions: Application to Benzenes, Pyridines, and DNA Bases. *J. Comput. Chem.* **2006**, *27* (4), 491–504.

(31) Johnson, E. R.; Keinan, S.; Mori-Sánchez, P.; Contreras-García, J.; Cohen, A. J.; Yang, W. Revealing Noncovalent Interactions. *J. Am. Chem. Soc.* **2010**, *132* (18), 6498–6506.

(32) Rozas, I.; Alkorta, I.; Elguero, J. Behavior of Ylides Containing N, O, and C Atoms as Hydrogen Bond Acceptors. *J. Am. Chem. Soc.* **2000**, *122* (45), 11154–11161.

(33) Emamian, S.; Lu, T.; Kruse, H.; Emamian, H. Exploring Nature and Predicting Strength of Hydrogen Bonds: A Correlation Analysis between Atoms-in-Molecules Descriptors, Binding Energies, and Energy Components of Symmetry-Adapted Perturbation Theory. *J. Comput. Chem.* **2019**, *40* (32), 2868–2881.

(34) Seo, A.; Jackson, J. L.; Schuster, J. V.; Vardar-Ulu, D. Using UV-Absorbance of Intrinsic Dithiothreitol (DTT) during RP-HPLC as a Measure of Experimental Redox Potential in Vitro. *Anal. Bioanal. Chem.* **2013**, *405*, 6379–6384.

(35) Marenich, A. V.; Cramer, C. J.; Truhlar, D. G. Universal Solvation Model Based on Solute Electron Density and on a Continuum Model of the Solvent Defined by the Bulk Dielectric Constant and Atomic Surface Tensions. *J. Phys. Chem. B* **2009**, *113* (18), 6378–6396.

(36) Lukesh III, J. C.; VanVeller, B.; Raines, R. T. Thiols and Selenols as Electron-Relay Catalysts for Disulfide-Bond Reduction. *Angew. Chem. Int. Ed.* **2013**, *52* (49), 12901–12904.

(37) Krężel, A.; Leśniak, W.; Jeżowska-Bojczuk, M.; M\lynarz, P.; Brasuñ, J.; Koz\lowski, H.; Bal, W. Coordination of Heavy Metals by Dithiothreitol, a Commonly Used Thiol Group Protectant. *J. Inorg. Biochem.* **2001**, *84* (1–2), 77–88.